Published in final edited form as:
Mol Cell. 2011 November 4; 44(3): 385–396. doi:10.1016/j.molcel.2011.08.036.

The structural basis for substrate recognition by mammalian polynucleotide kinase 3' phosphatase

Fernando Garces, **Laurence H. Pearl***, and **Antony W. Oliver***
Cancer Research UK DNA Repair Enzymes Group, Genome Damage and Stability Centre, School of Life Sciences, University of Sussex, Falmer, BN1 9QG, UK

Abstract

Mammalian polynucleotide kinase 3' phosphatase (PNK) plays a key role in the repair of DNA damage, functioning as part of both the non-homologous end-joining (NHEJ) and base-excision repair (BER) pathways. Through its two catalytic activities, PNK ensures that DNA termini are compatible with extension and ligation by either removing 3'-phosphates from, or by phosphorylating 5'-hydroxyl groups on, the ribose sugar of the DNA backbone. We have now determined crystal structures of murine PNK with DNA molecules bound to both of its active sites. The structure of ssDNA engaged with the 3'-phosphatase domain suggests a mechanism of substrate interaction that assists DNA end-seeking. The structure of dsDNA bound to the 5'-kinase domain reveals a mechanism of DNA bending that facilitates recognition of DNA-ends in the context of single-strand and double-strand breaks, and suggests a close functional cooperation in substrate recognition between the kinase and phosphatase active sites.

Keywords

nucleotide kinase; nucleotide phosphatase; DNA repair; catalytic mechanism

INTRODUCTION

Repair of DNA single-strand breaks and small gaps in mammalian cells is achieved in a short-patch repair pathway, organised around the protein XRCC1. This multi-domain 'scaffold' recruits and coordinates a DNA polymerase (Polβ) and DNA ligase (Lig3α) that respectively fill in missing nucleotides and restore the linkage of the phosphodiester backbone (Caldecott et al., 1996; Cappelli et al., 1997). The combination of these three proteins is sufficient for facile repair of defined DNA substrates *in vitro* (Kubota et al., 1996; Nash et al., 1997).

Single-strand breaks and gaps arise *in vivo*, as the result of a plethora of chemical and radiological insults. Many of these leave DNA ends lacking the free 3'-hydroxyl on one side of the gap, and 5'-phosphate group on the other, which respectively permit template-directed

*Corresponding authors: LH Pearl Tel.: + 44 1273 876544; Fax: + 44 1273 877586; laurence.pearl@sussex.ac.uk or AW Oliver Tel.: +44 1273 678349; Fax: +44 1273 678121; antony.oliver@sussex.ac.uk.

ACCESSION NUMBERS
Protein Databank **:** 3zvl, 3zvm, 3zvn

Europe PMC Funders Author Manuscripts

DNA synthesis and ATP-dependent ligation. In these circumstances DNA end-processing is required before SSB repair can be completed (Rass et al., 2007). 5'-hydroxyls and 3'-phosphates are common products of radiological damage to DNA, and are inimical to DNA polymerase and DNA ligase activity. Both of these blocking lesions can be repaired by the action of an unusual bifunctional DNA end-processing enzyme, polynucleotide kinase 3′ phosphatase (PNK or PNKP) that facilitates SSB repair by phosphorylating 5'-hydroxyls and/or dephosphorylating 3'-phosphates at the margins of DNA single-strand gaps (Habraken and Verly, 1983, 1986; Jilani et al., 1999; Mani et al., 2001). PNK is also recruited to the SSB repair complex by XRCC1; however unlike Polβ and Lig3α, the interaction is mediated by a multiply phosphorylated segment sited between the central and C-terminal BRCT domains, which provides a binding site for the N-terminal forkhead-associated (FHA) domain of PNK (Ali et al., 2009; Loizou et al., 2004; Whitehouse et al., 2001). A second, direct interaction of XRCC1 with the catalytic region of PNK may also play a role in regulating its enzymatic activity (Lu et al., 2010).

Previous structural studies have defined the overall architecture of this bi-functional enzyme, and revealed the details of its FHA-dependent interaction with XRCC1 (Ali et al., 2009; Bernstein et al., 2005). However there has been limited structural insight into how PNK actually recognises its different DNA substrates, and current models lack experimental support (Weinfeld et al., 2011). To address this deficit we have now determined structures of the catalytic region of murine PNK in complex with DNA in both the 3'-phosphatase and 5'-kinase active sites. The structures and associated mechanistic studies provide a comprehensive picture of DNA-end recognition by this dual function enzyme.

RESULTS

Substrate recognition by the phosphatase domain

Crystals of PNK with a ssDNA bound to the phosphatase domain were obtained by incubating a murine PNK construct lacking the N-terminal FHA domain (PNKΔFHA: amino acids 111-512) with DNA in a 1.5:1 DNA:protein ratio, in the presence of a ~10-fold excess of Mg^{2+}-ATP. Crystals appeared after a period of several weeks and were further soaked overnight in the precipitant, augmented with the ssDNA at 0.5mM, before cryoprotecting for data collection. Data were collected from a single soaked crystal, which diffracted to a resolution of 2.0Å (Table 1), and the structure was solved by molecular replacement (see Materials and Methods).

The difference maps from these crystals (Table 1 - PNK-DNA1) revealed the presence of a short stretch of single-stranded DNA bound to a narrow channel traversing the phosphatase domain (Figure 1A**,** Supplementary Figure S1). The channel also contained a well-ordered magnesium ion coordinated by the side chains of Asp170 and Asp288, along with the backbone carbonyl of Asp172 (Figure 1B). The location and coordination of the magnesium ion identifies it as the essential co-factor for the phosphatase activity based on analogy to other proteins of the haloacid dehalogenase (HAD) enzyme family, to which PNK-phosphatase domain is structurally related (Bernstein et al., 2005). Additionally, Mg^{2+}-ADP and a molecule of HEPES buffer are bound to the kinase active site (see below).

The three most 3' deoxynucleotides (C_3-A_4-C_5) of the single-stranded DNA are clearly visible in the channel. The bases of C_3 and A_4 are stacked against each other in van der Waals contact, and the stacked pair are themselves sandwiched between the side chains of Lys225 and Phe184 (Figure 1C). The interconnecting phosphate (5'P-A_4) is coordinated through a bi-dentate interaction with the guanidine head group of Arg258 and the backbone nitrogen of Met219 (Figure 1D). The terminal base (C_5) is not stacked contiguously with C_3 and A_4, but is instead rotated perpendicularly to the other bases to sit between the hydrophobic side-chains of Phe184 and Phe305 (Figure 1E). An oxygen atom of the phosphate bridging to A_4 makes a ligand interaction with the catalytic magnesium bound by Asp170, Asp172 and Thr216.

Based on studies of other phosphoester hydrolase enzymes in the haloalkane dehydrogenase family, PNK phosphatase is believed to operate via an SN2 reaction mechanism (Bernstein et al., 2005), in which the Mg^{2+} ion activates the terminal 3'-phosphate for nucleophilic attack, by Asp170 in the case of PNK, generating a carboxyl–phosphate ester intermediate, that is hydrolysed in the next stage of the mechanism. Comparison with the structure of a phospho-aspartate mimetic reaction intermediate of the HAD-family enzyme phosphoserine phosphatase, (Cho et al., 2001) (PDB: 1j97), suggests that the phosphatase active site is fully assembled and poised for catalysis. However the reaction cannot proceed as the bridging phosphate bound to the magnesium ion is not positioned correctly for hydrolysis due to the conformational restrictions imposed by its connection to the C_5 base stacked between Phe184 and Phe305 (Figure 1F). A *bona fide* 3'-terminal phosphate similarly located would be unencumbered and able to interact productively with the active site.

Rather than leading into a blind-ended pocket that would provide explicit selective binding of a 3'-phosphorylated terminus, the phosphatase channel is open-ended and could provide favourable backbone interactions with segments of ssDNA 3' to the active site. Thus, although its catalytic activity is restricted to terminal 3'-phosphates, PNK appears to be fully capable of binding non-terminal segments of ssDNA. The combination of the phosphate backbone interactions made by Arg258, the phosphate contact made by the catalytic magnesium ion, and the base stacking interaction provided by Phe184 and Phe305, would allow isoenergetic sliding of ssDNA segments through the channel. This would facilitate location of 3'-phosphate ends on extended 3'-overhanging substrates such as those generated in double-strand break resection by DNA2 or EXO1 in collaboration with BLM, RPA and the MRN complex, as part of the homologous recombination pathway of DNA-repair (Gravel et al., 2008; Mimitou and Symington, 2008; Nimonkar et al., 2011; Zhu et al., 2008).

While the DNA backbone and base-stacking interactions are generic and impose no significant DNA sequence specificity on the phosphatase activity, they are totally incompatible with the 3'-phosphorylated substrate DNA strand remaining base paired. The requirement for ssDNA in the phosphatase channel does imply that PNK must be able to facilitate a substantial local disruption of DNA base-pairing when the substrate 3'-phosphorylated end is presented in the context of a gapped or nicked DNA duplex (see below).

As there has been no previous experimental observation of DNA bound to a polynucleotide 3'-phosphatase, we were concerned to confirm the role of the amino acids implicated in recognition and hydrolysis by our crystal structure.

We therefore generated a series of mutants within the phosphatase domain of PNKΔFHA, and determined their ability to bind DNA using an electrophoretic mobility shift assay (EMSA), and their catalytic activity using a fluorescent gel-based assay (Dobson and Allinson, 2006) (Figure 2A,B).

As expected, incubation of the single-stranded oligonucleotide FAM1 (see Materials and Methods) with increasing concentrations of wild-type PNKΔFHA resulted in rapid removal of the 3' phosphate, visualised by the decrease in electrophoretic mobility of the fluorescent oligonucleotide on denaturing polyacrylamide gels. A charge-reversal mutation of Arg258 to a glutamic acid (R285E) resulted in a substantial decrease in phosphatase activity, consistent with a key role in binding the phosphodiester backbone of the 5'-GTCAC-3' oligonucleotide substrate, as indicated by the crystal structure (Figure 1D). An F184G mutation, which removes the favourable stacking interaction between A_4 and the side-chain of Phe184 had minimal effect in isolation, but combined with the R258E mutation, substantially reduced phosphatase activity at all but the highest enzyme concentrations.

Studies of the mono-functional *S.cerevisiae* DNA 3'-phosphatase Tpp1, to which the 3'-phosphatase domain of mammalian PNK is homologous, have implicated a key aspartic acid residue (Asp 35) as both a ligand for the catalytically essential Mg^{2+} co-factor, and as the phosphate acceptor in the covalent mechanism (Deshpande and Wilson, 2004). Consistent with this, mutation of the equivalent residue in human PNK (Asp 171) to alanine resulted in complete loss of phosphatase activity (Dobson and Allinson, 2006). We made a D170N mutation in murine PNK and assayed its DNA binding and phosphatase activity as above, as expected, PNK-D170N was virtually catalytically inactive, however unlike the F184A/R258E mutant, its ability to bind ssDNA was essentially wild-type (Figure 2C).

Substrate recognition by the kinase domain

Despite extensive trials, we were unable to obtain PNK crystals with DNA bound at the kinase active site using the wild-type protein and conventional nicked dsDNA substrates generated by annealing three separate oligonucleotides. We therefore tried a number of alternative strategies culminating in incubation of phosphatase-dead PNK-D170N with a 10-fold excess of ssDNA oligonucleotide and ATP, in the presence of Mn^{2+} rather than Mg^{2+}. In this way we obtained a new crystal form diffracting to 2.2Å, in which DNA was evidently bound in the kinase domain (Figure 3A**,** Supplementary Figure S2).

These crystals (PNK-DNA2) contain a single copy of PNK-D170N in the asymmetric unit, associated with five copies of the ssDNA 5'-GTCAC-3'. The oligonucleotides are annealed to each other to form a self-complementary blunt-ended duplex with a central C:C mismatch (DNA-A* / DNA-B*) and a nicked-duplex structure in which one 5'-GTCAC-3' oligonucleotide (DNA-A) is base-paired to a second oligonucleotide (DNA-B) via the 5'-GTC sequence, and to a third (DNA-C) via the AC-3' sequence. The exposed base-pairs at the end of the duplex segments stack on each other and on symmetry related duplex ends to

Europe PMC Funders Author Manuscripts

form pseudo-continuous DNA duplexes that builds the crystal lattice (Supplementary Figure S3).

The 5'-nucleotide (G*) of DNA-B lies adjacent to a pocket in the kinase domain of PNK flanked by α-helices 8 and 12 (using the nomenclature and numbering described in (Bernstein et al., 2005)). In the DNA complex the pocket is occupied by an ADP molecule and the 5'-OH of G* (and all other visible 5'-ends) is phosphorylated, suggesting that the enzyme has turned over during crystallogenesis and that the crystals contain a product complex. Fluorescence-based kinase assays confirmed that the PNK-D170N enzyme has essentially the same activity when either magnesium or manganese is provided as a co-factor (see Supplementary Figure S4)

Within this pocket N1 and N6 of the adenine ring are hydrogen-bonded to the backbone carbonyl and peptide NH of Arg503 and Gln505 respectively (Figure 3B), in a similar manner to the 'hinge' binding observed in protein kinases (Johnson et al., 1996; Noble et al., 2004). Hydrophobic residues Ile345, Phe462, Phe502, Leu504, Leu508 and Tyr516 form the walls of the adenine pocket. The Oγ of Thr466, coordinates the O3' position of the ribose moiety through a water-mediated interaction (Figure 3C). Numerous polar interactions occur between ADP phosphate oxygens and the protein (Figure 3D), including extensive backbone contacts with NH groups of the Walker A / P-loop motif 374-GAGKST-379. Additional interactions are provided by the side-chains and peptide NH groups of Lys377, Ser378 and Thr379, and the guanidinium head group of Arg463.

A Mn^{2+}-ion and associated solvent bridges the side chain of Ser378 and the β-phosphate of the ADP to the 5'-phosphate of the DNA-B strand and the carboxylate side chain of Asp396 (Figure 3E). Arg395, which hydrogen bonds to the phosphate group on the 3'-side of the 5'-guanine, also interacts with Asp396, orientating its carboxylate group towards what would have been the terminal 5'-OH of the DNA strand. The 5'-phosphate group receives a hydrogen bond from the imidazole side chain of His470. Based on their position and interactions in the product complex Asp396 is well placed to act as a general base in the phosphoryl transfer reaction, abstracting a proton from the 5'-OH of the DNA, consistent with the significant loss of activity observed when this residue is mutated to asparagine (Bernstein et al., 2009).

Recognition of Strand Discontinuity by PNK

The 5'-phosphorylated guanine bound in the active site, as well as the two bases 3' to that in the DNA-B molecule, are fully base paired to the DNA-A molecule. The conformation of the base-paired segment is essentially canonical B-form DNA (very slightly perturbed by the central T:T mismatch) and could continue unimpeded as linear duplex DNA beyond that (Figure 4A). The phosphate backbone of the continuous strand makes no contact with the protein, but the backbone of the discontinuous strand lies in a shallow basic channel with the phosphates for the three nucleotides upstream of the 5'-nucleotide interacting with side chains of Arg395, Arg432 and Trp401. The exposed face of the base-pair formed by the 5'-phosphorylated guanine and its cytosine partner, packs against an extended hydrophobic platform, generated by the side chains of Pro373 and Val473, and by Met476 and Val477 at

Europe PMC Funders Author Manuscripts

the N-terminal end of helix α13, whose axis runs perpendicular to the axis of this segment of duplex DNA.

The insertion of helix α13 into the path of the duplex DNA, completely blocks any possibility of maintaining base stacking on either strand, across the site of the nick. Instead, the backbone of the continuous strand undergoes a substantial change in direction, folding around the surface of α13, with the 3'-AC bases resuming base-pairing with the 5'-end of a third oligonucleotide (DNA-C). As with the last base-pair on the 5'-side of the nick, the exposed face of the first base-pair on the 3'-side packs against a hydrophobic surface formed by Met476, Phe479 and Ser480 from α-helix 13, with Arg482 and Lys483 providing polar interactions for the phosphate backbone as it twists around the surface of α13 (Figure 4B).

To determine the significance of the interactions provided by α13 we mutated Val477, to disrupt the hydrophobic interface with the exposed base-pair surface, and Arg482 and Lys 483, to disrupt the phosphate backbone interactions (in the context of the phosphatase-dead PNK-D170N protein). Compared to the wild-type amino-acids, V477R and R482E, and K483E mutations significantly diminished the ability of the enzyme to phosphorylate a 5'-OH in the context of a nicked duplex (Figure 5A,B). The substantial reduction in kinase activity observed for these mutants confirms the biological significance of the interactions observed in the crystal structure, and defines a key role for the α13-helix in exposing and positioning the 5'-substrate in the kinase active site.

Although only two base-pairs of duplex are formed in the crystals beyond α13, the conformation of these is almost perfect B-form, and there is no obstacle to the DNA continuing as a linear duplex beyond this (Figure 6A,B), potentially making favourable electrostatic interactions with a number of extended basic loops (involving lysines 182, 225, 301, 302 and 303) on the surface of the phosphatase domain. Thus the phosphatase domain may play a role in assisting the kinase domain in its activity towards nicked and gapped substrates.

The 3'-nucleotides on DNA-C 3' not involved in base-pairing with DNA-A, curl into the mouth of the ssDNA-binding channel we identify in the phosphatase domain (see above), with the bases of the two most 3' nucleotides occupying the base-stacking sites between Lys225 and Phe184 and between Phe184 and Phe305 (Figure 3A, Figure 7A-B). As in the complex with ssDNA, Arg258 interacts with the phosphate backbone, but in this case with the phosphate 5' of the 3'-terminal nucleotide. While no catalytic metal is present due to the D170N mutation, and the terminal nucleotide carries a 3'-OH, the position of the terminal base suggests that were a 3' phosphate present, it would be able to interact productively with the active site. Thus, the two active sites in PNK appear to be simultaneously able to make productive contact with their cognate end-chemistries within the same DNA substrate.

Induced-Fit in the PNK kinase domain

Comparison of the PNK-kinase DNA complex and an apo-structure of PNK determined at 1.6Å resolution (see Materials and Methods) shows a number of structural rearrangements in the kinase domain that accompany binding to DNA and ADP (Supplementary Figure S5). Strand β16, helices α9 and α10, and their connecting loops, swing towards the centre of the protein, hinging at Gly389 and Gly415. This movement establishes a cluster of direct and water-bridged interactions with the phosphate backbone of the nicked strand, involving Trp401, Gln402 and Arg395, and moves the catalytic Asp396 ~ 5Å from its position in the apo-structure to lie above the 5'-oxygen of the terminal nucleotide (FIGURE 7C). A second more subtle rearrangement occurs in the loop carrying the amino acid His470, and the hinge segment at residues 503-508, which open out to accommodate and interact with the ADP/ATP (FIGURE 7D).

The observed differences between the apo and substrate — bound kinase domain structures are compatible with solution circular dichroism and UV-difference spectroscopy studies (Mani et al., 2001) that indicated a conformational change on binding ATP to human PNK. Thus the DNA 5'-kinase domain of PNK appears to display active and inactive conformations, which are reminiscent of the active and inactive conformations that mediate allosteric regulation of protein kinases (Johnson et al., 1996). Recent observations suggest that the DNA 5'-kinase activity of PNK may also be subject to allosteric activation via direct interaction with the XRCC1 scaffold protein (Lu et al., 2010), but whether this is mediated by the conformational flexibility of the β16-α9-α10 segment, is currently unknown.

DISCUSSION

Gap Recognition and DNA Distortion

The crystal structures presented here provide a definitive view of the interaction of PNK with both of its DNA substrates, and fully explain the distinctive and individual specificities of the phosphatase and kinase functions. The phosphatase active site lies within a narrow channel that precludes binding of duplex DNA. This explains the observation that *in vitro* PNK preferentially dephosphorylates single-stranded DNA or duplex DNA substrates with at least a three nucleotide 3'-overhang (Bernstein et al., 2005). Nonetheless, PNK *in vivo* must also act on 3'-phosphates in the context of single-strand gaps and double-strand breaks, so that it must be able to stabilise unstacking of the bases and local unwinding of the DNA in the vicinity of a strand discontinuity in order to access a 3'-end.

By contrast, the DNA-binding site in the kinase domain readily accommodates undistorted duplex DNA upstream of the site of the 5'-terminus bound in the active site. However, the chemistry of phospho-transfer from ATP bound in the co-factor pocket of the kinase domain, requires all-round access to the 5'-terminal hydroxyl group that is not possible in the context of a fully stacked DNA duplex. Thus, as for the 3'-phosphatase function, the 5'-kinase function requires PNK to stabilise unstacking of the duplex DNA for substrates in which the 5-OH is presented in the context of a nick or small gap. For both enzymatic functions, the necessary DNA distortion is provided by helix α13, which inserts into the DNA providing a two-sided hydrophobic 'wedge' to support the exposed base-pair surfaces from both phosphatase and kinase substrates, and charged interactions to stabilise the distorted path of the sugar-phosphate backbone of the continuous strand that connects the two. The ~70° bend observed in the path of the DNA as it traverses the adjacent active sites, was not predicted by previous low-resolution analysis and the orientation of the duplex DNA as it engages with the kinase active site, is significantly different to models for DNA interaction by PNK suggested on the basis of those studies (Bernstein et al., 2009).

Europe PMC Funders Author Manuscripts

Functional coupling of 3’-phosphatase and 5’-kinase domains

The presence of two distinct enzymatic activities in PNK has always raised the tantalising possibility that their functions might in some way be coupled. Certainly many DNA damage events generating single-strand gaps or double-strand breaks can produce both 3’-phospho and 5’-hydoxyl ends, requiring both of PNK’s catalytic activities for repair. The DNA complex presented here provides a composite view of the binding modes of substrate DNA ends for both enzymatic functions within a single complex. The duplex segments define a clear trajectory for DNA substrates with nicks and short gaps, which are by far the most common substrates for PNK *in vivo*. A single common binding mode for nicked/gapped DNAs that facilitates access to either active site, fully explains the intriguing observation that binding of 3’-phosphorylated substrates to a D171A phosphatase-dead human PNK mutant, is inhibitory of the 5’-kinase activity towards gapped duplex DNA (Dobson and Allinson, 2006). This common binding mode would allow either active site to readily access a range of DNA double-strand break substrates, in whose repair by the non-homologous end-joining system PNK also play an important role.

The structures presented here explain how the composite domain structure of PNK utilises a single DNA binding mode to achieve two different enzymatic reactions required to facilitate single-strand gap break repair. PNK is however only one of at least four enzymes known to be associated with the XRCC1-scaffolded short-patch repair complex, all of which require access to DNA ends for their function. How these competing requirements for end-access by APTX, Polβ, Lig3β and PNK are coordinated and regulated, remains one of the major challenges in understanding the structural basis for single-strand gap repair.

MATERIALS AND METHODS

Cloning, expression and purification of PNKΔFHA

An *E.coli* codon-optimised sequence for full-length murine PNK was generated by gene synthesis (Eurofins Medigenomix, Martinsried, Germany). PCR primers were then used to amplify the region encoding the phosphatase and kinase domains (PNKΔFHA; amino acids 111-522) with additional flanking restriction sites (*Nde*I and *Eco*RI) to allow cloning into the vector pTWO-E; an in-house modified pET-17b vector (Novagen, Nottingham, UK) engineered to encode an N-terminal, 3C-Protease cleavable, His_6 affinity tag.

The recombinant plasmid was transformed into the *E.coli* strain Rosetta2(DE3) pLysS (Merck Chemicals, Nottingham, UK). A 250 ml flask containing 100 ml of L-broth (1% w/v tryptone, 0.5% w/v NaCl, 0.5% w/v yeast extract), supplemented with 100 μg/ml ampicillin and 34 μg/ml chloramphenicol, was inoculated with a single transformed bacterial colony. This was grown, overnight, in an orbital incubator set at 37 °C and 225 rpm. From this ‘starter culture’, 10 ml was then used to inoculate a 2 l flask containing 1 l of L-broth supplemented, as before, with antibiotics. The culture was grown in an orbital incubator set at 37 °C and 225 rpm. Once the A600 of the cell culture had reached 0.6, the incubator temperature was reduced to 20 °C and expression of PNKΔFHA induced by the addition of IPTG to a final concentration of 0.5 mM. The culture was grown for a further 16-18 hours at

20 °C, after which the cells were harvested by centrifugation (3100 g, 10 minutes, 10 °C), and the pellet stored at −80 °C until required.

The pellet arising from 10 l of cell culture was resuspended in 150 ml of buffer A: 50 mM HEPES-HCl pH 7.4, 1000 mM NaCl, 0.5 mM TCEP supplemented with protease inhibitor tablets (Roche, Burgess Hill, UK). The cells were lysed by sonication, after which cell debris and insoluble material were removed by centrifugation at 40 000 × *g* for 30 min at 4 °C. The supernatant arising from this step was applied to a batch/gravity column containing 10 ml of Talon affinity resin (TaKaRa Bio, Saint-Germain-en-Laye, France) equilibrated in Buffer A. The column containing the cell extract and resin was rotated/rolled at 4 °C for a period of 1 hour to facilitate protein binding. The resin was allowed to pack under gravity, and then washed with successive applications of Buffer A (approximately 250 ml in total). Any retained protein was eluted from the column with the application of Buffer B: 50 mM HEPES-HCl pH 7.4, 1000 mM NaCl, 0.5 mM TCEP, 300 mM imidazole. Fractions containing PNKΔFHA were pooled, then concentrated to a final volume of 10 ml using Vivaspin 20 (5000 MWCO) centrifugal concentrators (Sartorius Stedim Biotech, Goettingen, Germany) before loading onto a HiLoad Superdex 75 size exclusion column (GE Healthcare, Little Chalfont, UK) equilibrated with Buffer C: 50 mM HEPES-HCl pH 7.4, 500 mM NaCl, 0.5 mM TCEP. Fractions containing PNKΔFHA were again identified by SDS-PAGE, then pooled and concentrated as before. The affinity tag was cleaved from the protein by incubation with rhinovirus 3C-protease overnight at 4°C (PreScission protease, GE Healthcare), before being passed back through a Talon batch/gravity column (to remove any uncleaved protein and the residual tag), then reapplied to a S75 size exclusion column, equilibrated this time in Buffer D: 10 mM HEPES-HCl pH 7.4, 100 mM NaCl, 0.5 mM TCEP. Fractions containing the purified protein were identified, and then concentrated to 20 mg/ml, where it was either stored at 4°C for immediate use, or flash-frozen on dry-ice then stored at −80°C until required.

Crystallisation, Data Collection and Phasing

PNK-apo—Crystallisation trials were carried out using the vapour-diffusion method in MRC 2 sitting-drop crystallisation plates, at a 20 mg/ml concentration of PNKΔFHA, a temperature of 4 °C, and by mixing 200 nl of protein with 200 nl of the precipitant solution with diffusion against a well volume of 50 μl. Crystals were observed only after an extended incubation period (~ 7 months) in condition C3 of the Nucleix Suite (Qiagen, Crawley, UK): 0.05 M Na.Cacodylate pH 6.5, 0.2 M Ammonium acetate, 0.01 M Mg acetate, 30 % (w/v) PEG 8000. Crystals were cryoprotected for data collection by step-wise soaking in buffers containing increasing amounts of glycerol, to a final concentration of 30% (v/v). No further optimisation was necessary.

Diffraction data were collected to 1.65 Å on station I03 at the Diamond Light Source, Didcot, UK. Data were integrated and scaled using the software packages iMosflm (Leslie, 1995) and Scala / ctruncate from the CCP4 suite (CCP4, 1994).

The protein crystallised in spacegroup $P2_1$ with unit-cell dimensions a = 42.8 Å; b = 63.5 Å; c = 67.9 Å; β =91.8° with a single molecule comprising the asymmetric unit. Statistics for the data collection are given in Table 1.

PNK-DNA1—PNKΔFHA at 20 mg/ml (0.47 mM) was combined with 0.75 mM oligonucleotide (5’-GTCAC-3’; Eurofins MWG Operon, Ebersberg, Germany) and 10 mM ATP (from a stock solution of 50 mM ATP, 50 mM $MgCl_2$ and 100 mM Tris-HCl pH 7.5), then incubated at 4°C for a period of 3-4 hours. Crystallisation trials were then undertaken using the same methodology and format as that described for PNKΔFHA.

Crystals were observed only after ~3 weeks in condition F4 of the Protein Complex Suite (Qiagen, Crawley, UK): 0.1M HEPES pH 7.0 and 18% (w/v) PEG 12000.

Crystals were then transferred into a 5 µl drop containing condition F4, supplemented with 0.5 mM of the 5’-GTCAC-3’ oligonucleotide. The crystals were soaked overnight at 4°C and then cryoprotected as before.

Diffraction data were collected to 2.0 Å ‘in-house’ on a Bruker AXS Microstar H rotating anode. Data were processed and scaled using the manufacturer-supplied PROTEUM software suite and XPREP (Sheldrick, 2008).

The complex crystallized in the spacegroup $P2_1$ with unit-cell dimensions of a = 44.9 Å, b = 75.2 Å, c = 135.2 Å, β = 96.3°, with two molecules comprising the asymmetric unit. Statistics for the data collection are given in Table 1.

PNK-DNA2—PNKΔFHA(D170N) at 20 mg/ml (0.47 mM) was combined with 4.4 mM oligonucleotide (5’-GTCAC-3’) and 10 mM ATP (from a stock solution of 50 mM ATP, 50 mM $MnCl_2$ and 100 mM Tris-HCl pH 7.5), then incubated at 4°C for a period of 3-4 hours. Crystallisation trials were then undertaken using the same methodology and format as that described for PNKΔFHA.

Crystals were observed at 4°C after 3-5 days in condition H6 of the JSCG+ screen (Molecular Dimensions, Suffolk, UK): 0.1 M Bis Tris pH 5.5, 0.1 M Ammonium acetate, 17 % (w/v) PEG 10000. Crystals were cryoprotected for data collection by step-wise soaking in buffers containing increasing amounts of glycerol, to a final concentration of 30% (v/v). No further optimisation was necessary.

Diffraction data were collected to 2.15Å on station I02 at the Diamond Light Source, Didcot, UK. Data were integrated and scaled as for PNK-apo.

The protein crystallised in spacegroup $P2_12_12_1$ with unit-cell dimensions a = 69.3 Å; b = 73.0 Å; c = 114.4 Å, with a single molecule comprising the asymmetric unit.

Phasing and Refinement—In each case, a solution was determined by molecular replacement using PHASER (McCoy, 2007) with the previously reported murine PNK structure (PDB: 1YJ5) as a search model. Iterative cycles of refinement (PHENIX; (Adams et al., 2002) and manual intervention (Coot; (Emsley and Cowtan, 2004)) gave the final models. Refined coordinates and structure factors have been deposited in the Protein Databank as: 3zvl (PNK-apo), 3zvm (PNK-DNA1 and 3zvn (PNK-DNA2).

Oligonucleotides—Fluorescently-labelled oligonucleotides were purchased from Eurofins MWG Operon (Ebersberg, Germany). The sequences (5' to 3') of the oligonucleotides used are: FAM1: (FAM)-TAGCATCGATCAGTCCTCp; FAM2: (FAM)-TAGCATCGATCAGTCCTC; FAM3: TAGCATCGATCAGTCCTC; TAMRA: GAGGTCTAGCATCGTTAGTCA-(TAMRA); COMP1: TGACTAACGATGCTAGACCTCGAGGACTGATCGATGCTA

Phosphatase and Kinase Assays—Assays were carried out using the protocol previously described by Dobson and Allinson (Dobson and Allinson, 2006).

For the phosphatase assays, FAM1 (8 nM) was incubated with the indicated concentrations of wild-type or mutant PNKΔFHA for 10 minutes at 37 °C. Reactions typically took place in a sample volume of 10 μl, containing 50 mM MES pH 6.0, 10 mM $MgCl_2$ and 0.5 mM TCEP, and were stopped by the addition of 10 μl of formamide loading buffer (10 mM EDTA, 98% formamide, 10 mg/ml blue dextran) and incubation at 95 °C for a period of 3 minutes. Samples were analysed on a 20% denaturing polyacrylamide gel, and visualized by fluorimagery using a Typhoon 9410 laser scanning system (GE Healthcare). All experiments were repeated at least three times. Image straightening has been used for presentation purposes only, in order to correct 'smiling' gel artefacts, using the 'Straighten' plugin (Kocsis et al., 1991) available for ImageJ. Band intensities were measured using ImageJ (Abramoff et al., 2004). The amount of product generated in each case was calculated as the intensity of the product band as a proportion of the total intensity of the product and substrate bands.

For the kinase assays, a nicked DNA substrate was prepared by annealing the three oligonucleotides FAM3, TAMRA and comp1. DNA (at 15 nM) was then incubated with increasing concentrations of PNK(D170N) or selected mutants for 10 minutes at 37 °C.

Reactions typically took place in a sample volume of 10 μl, containing 50 mM MES pH 6.0, 20 mM NaCl, 10 mM $MgCl_2$, 0.1 mM ATP and 0.5 mM TCEP, then stopped and analysed on a denaturing polyacrylamide gel as per the phosphatase assay. Gels were visualised by fluorimagery using an FLA-5100 laser scanning system (Fujifilm UK Ltd, Bedford, UK). All experiments were repeated at least three times. Band intensities were measured using the AIDA software package (Raytest GmbH, Germany). The amount of product generated in each case was calculated as the intensity of the product band as a proportion of the total intensity of the product and substrate bands.

EMSA—For electrophoretic mobility shift assays, oligonucleotide (5 μM) was incubated with increasing amounts of wild-type or mutant PNKΔFHA, on ice, for a period of 10 minutes. Samples were analysed on 5% v/v native polyacrylamide gels containing 0.5 × TBE buffer and 10% (v/v) glycerol, and visualised by fluorimagery as before.

Supplementary Material

Refer to Web version on PubMed Central for supplementary material.

Europe PMC Funders Author Manuscripts

ACKNOWLEDGEMENTS

We would like to thank Mark Roe for his assistance in data collection and processing. We are grateful to the Diamond Light Source, Didcot, UK for access to synchrotron radiation. This work was supported by Cancer Research UK Programme grant C302/A8265 and Infrastructure Support grant C302/A7803 to L.H.P.

REFERENCES

Abramoff MD, Magelhaes PJ, Ram SJ. Image Processing with ImageJ. Biophotonics International. 2004; 11:36–42.

Adams PD, Grosse-Kunstleve RW, Hung LW, Ioerger TR, McCoy AJ, Moriarty NW, Read RJ, Sacchettini JC, Sauter NK, Terwilliger TC. PHENIX: building new software for automated crystallographic structure determination. Acta Crystallogr D Biol Crystallogr. 2002; 58:1948–1954. [PubMed: 12393927]

Ali AA, Jukes RM, Pearl LH, Oliver AW. Specific recognition of a multiply phosphorylated motif in the DNA repair scaffold XRCC1 by the FHA domain of human PNK. Nucleic Acids Res. 2009; 37:1701–1712. [PubMed: 19155274]

Bernstein NK, Hammel M, Mani RS, Weinfeld M, Pelikan M, Tainer JA, Glover JN. Mechanism of DNA substrate recognition by the mammalian DNA repair enzyme, Polynucleotide Kinase. Nucleic Acids Res. 2009; 37:6161–6173. [PubMed: 19671525]

Bernstein NK, Williams RS, Rakovszky ML, Cui D, Green R, Karimi-Busheri F, Mani RS, Galicia S, Koch CA, Cass CE, et al. The molecular architecture of the mammalian DNA repair enzyme, polynucleotide kinase. Mol Cell. 2005; 17:657–670. [PubMed: 15749016]

Caldecott KW, Aoufouchi S, Johnson P, Shall S. XRCC1 polypeptide interacts with DNA polymerase beta and possibly poly (ADP-ribose) polymerase, and DNA ligase III is a novel molecular ‘nick-sensor’ in vitro. Nucleic Acids Res. 1996; 24:4387–4394. [PubMed: 8948628]

Cappelli E, Taylor R, Cevasco M, Abbondandolo A, Caldecott K, Frosina G. Involvement of XRCC1 and DNA ligase III gene products in DNA base excision repair. J Biol Chem. 1997; 272:23970–23975. [PubMed: 9295348]

CCP4. Programs for protein crystallography. Acta Crystallogr. 1994; D50:760–763.

Cho H, Wang W, Kim R, Yokota H, Damo S, Kim SH, Wemmer D, Kustu S, Yan D. BeF(3)(−) acts as a phosphate analog in proteins phosphorylated on aspartate: structure of a BeF(3)(−) complex with phosphoserine phosphatase. Proc Natl Acad Sci U S A. 2001; 98:8525–8530. [PubMed: 11438683]

Delano, WL. The PyMOL Molecular Graphics System. http://www.pymol.org

Deshpande RA, Wilson TE. Identification of DNA 3′-phosphatase active site residues and their differential role in DNA binding, Mg2+ coordination, and catalysis. Biochemistry. 2004; 43:8579–8589. [PubMed: 15222769]

Dobson CJ, Allinson SL. The phosphatase activity of mammalian polynucleotide kinase takes precedence over its kinase activity in repair of single strand breaks. Nucleic Acids Res. 2006; 34:2230–2237. [PubMed: 16648365]

Emsley P, Cowtan K. Coot: model-building tools for molecular graphics. Acta Crystallogr D Biol Crystallogr. 2004; 60:2126–2132. [PubMed: 15572765]

Gravel S, Chapman JR, Magill C, Jackson SP. DNA helicases Sgs1 and BLM promote DNA double-strand break resection. Genes Dev. 2008; 22:2767–2772. [PubMed: 18923075]

Habraken Y, Verly WG. The DNA 3′-phosphatase and 5′-hydroxyl kinase of rat liver chromatin. FEBS Lett. 1983; 160:46–50. [PubMed: 6309567]

Habraken Y, Verly WG. Chromatin 3′-phosphatase/5′-OH kinase cannot transfer phosphate from 3′ to 5′ across a strand nick in DNA. Nucleic Acids Res. 1986; 14:8103–8110. [PubMed: 3022244]

Jilani A, Ramotar D, Slack C, Ong C, Yang XM, Scherer SW, Lasko DD. Molecular cloning of the human gene, PNKP, encoding a polynucleotide kinase 3′-phosphatase and evidence for its role in repair of DNA strand breaks caused by oxidative damage. J Biol Chem. 1999; 274:24176–24186. [PubMed: 10446192]

Johnson LN, Noble ME, Owen DJ. Active and inactive protein kinases: structural basis for regulation. Cell. 1996; 85:149–158. [PubMed: 8612268]

Kocsis E, Trus BL, Steer CJ, Bisher ME, Steven AC. Image averaging of flexible fibrous macromolecules: the clathrin triskelion has an elastic proximal segment. J Struct Biol. 1991; 107:6–14. [PubMed: 1817611]

Kubota Y, Nash RA, Klungland A, Schar P, Barnes DE, Lindahl T. Reconstitution of DNA base excision-repair with purified human proteins: interaction between DNA polymerase beta and the XRCC1 protein. EMBO J. 1996; 15:6662–6670. [PubMed: 8978692]

Leslie, AGW. MOSFLM Users Guide. MRC Laboratory of Molecular Biology; Cambridge, UK: 1995.

Loizou JI, El-Khamisy SF, Zlatanou A, Moore DJ, Chan DW, Qin J, Sarno S, Meggio F, Pinna LA, Caldecott KW. The protein kinase CK2 facilitates repair of chromosomal DNA single-strand breaks. Cell. 2004; 117:17–28. [PubMed: 15066279]

Lu M, Mani RS, Karimi-Busheri F, Fanta M, Wang H, Litchfeld DW, Weinfeld M. Independent mechanisms of stimulation of polynucleotide kinase/phosphatase by phosphorylated and non-phosphorylated XRCC1. Nucleic Acids Res. 2010; 38:510–521. [PubMed: 19910369]

Mani RS, Karimi-Busheri F, Cass CE, Weinfeld M. Physical properties of human polynucleotide kinase: hydrodynamic and spectroscopic studies. Biochemistry. 2001; 40:12967–12973. [PubMed: 11669634]

McCoy AJ. Solving structures of protein complexes by molecular replacement with Phaser. Acta Crystallogr D Biol Crystallogr. 2007; 63:32–41. [PubMed: 17164524]

Mimitou EP, Symington LS. Sae2, Exo1 and Sgs1 collaborate in DNA double-strand break processing. Nature. 2008; 455:770–774. [PubMed: 18806779]

Nash RA, Caldecott KW, Barnes DE, Lindahl T. XRCC1 protein interacts with one of two distinct forms of DNA ligase III. Biochemistry. 1997; 36:5207–5211. [PubMed: 9136882]

Nimonkar AV, Genschel J, Kinoshita E, Polaczek P, Campbell JL, Wyman C, Modrich P, Kowalczykowski SC. BLM-DNA2-RPA-MRN and EXO1-BLM-RPA-MRN constitute two DNA end resection machineries for human DNA break repair. Genes Dev. 2011; 25:350–362. [PubMed: 21325134]

Noble ME, Endicott JA, Johnson LN. Protein kinase inhibitors: insights into drug design from structure. Science. 2004; 303:1800–1805. [PubMed: 15031492]

Potterton L, McNicholas S, Krissinel E, Gruber J, Cowtan K, Emsley P, Murshudov GN, Cohen S, Perrakis A, Noble M. Developments in the CCP4 molecular-graphics project. Acta Crystallogr D Biol Crystallogr. 2004; 60:2288–2294. [PubMed: 15572783]

Rass U, Ahel I, West SC. Defective DNA repair and neurodegenerative disease. Cell. 2007; 130:991–1004. [PubMed: 17889645]

Sheldrick GM. A short history of SHELX. Acta Crystallogr A. 2008; 64:112–122. [PubMed: 18156677]

Weinfeld M, Mani RS, Abdou I, Aceytuno RD, Glover JN. Tidying up loose ends: the role of polynucleotide kinase/phosphatase in DNA strand break repair. Trends Biochem Sci. 2011

Whitehouse CJ, Taylor RM, Thistlethwaite A, Zhang H, Karimi-Busheri F, Lasko DD, Weinfeld M, Caldecott KW. XRCC1 stimulates human polynucleotide kinase activity at damaged DNA termini and accelerates DNA single-strand break repair. Cell. 2001; 104:107–117. [PubMed: 11163244]

Zhu Z, Chung WH, Shim EY, Lee SE, Ira G. Sgs1 helicase and two nucleases Dna2 and Exo1 resect DNA double-strand break ends. Cell. 2008; 134:981–994. [PubMed: 18805091]

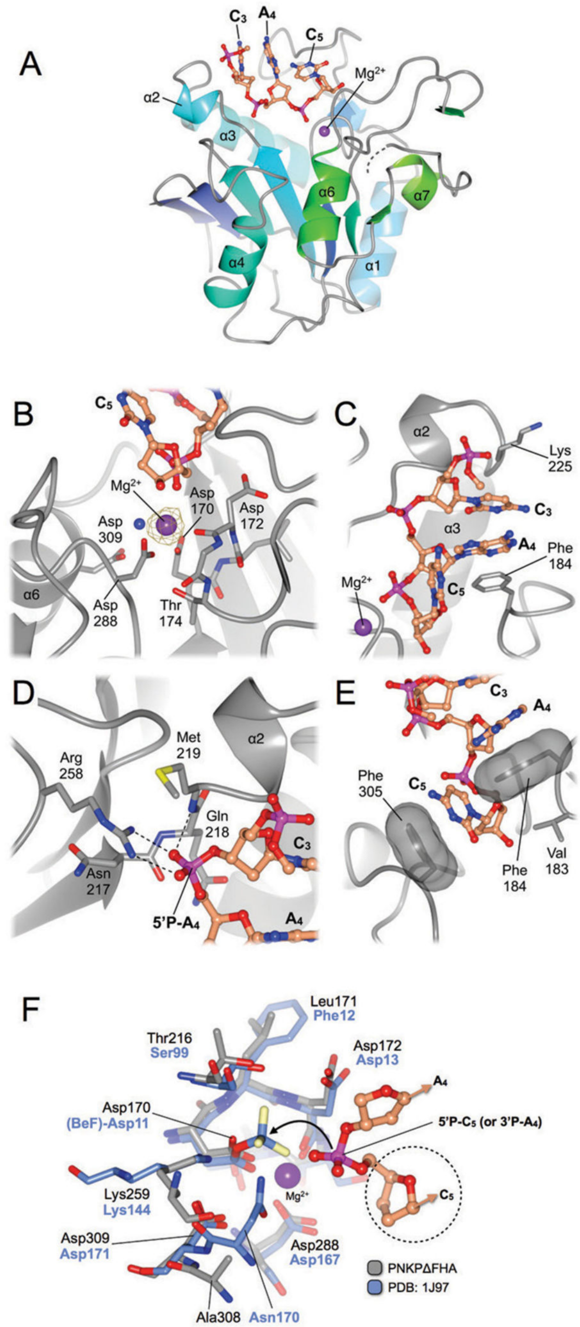

Figure 1. Structural details for single-stranded DNA bound to the phosphatase domain

(A) Secondary structure cartoon representation of the phosphatase domain in complex with a short single-stranded oligonucleotide (PNK-DNA1). **(B)** Coordination of the magnesium ion co-factor by the side-chains of Asp170, Asp288, the backbone carbonyl of Asp172, and through a water-mediated interaction with Asp309. Representative electron density, for the region surrounding the magnesium ion from an mF_{obs}-DF_{calc} omit map, is shown as a brown mesh contoured at 1.8σ. **(C)** The bases C3 and A4 of the bound oligonucleotide are stacked against each other, and sandwiched between the side-chains of Lys255 and Phe184. **(D)** The phosphate group (5’-P-A_4) connecting bases C3 and A4 is contacted by the head-group of Arg258, and the backbone nitrogen of Met219. **(E)** The terminal base of the oligonucleotide is not stacked contiguously with the other bases, but rotated perpendicularly to sit between the side-chains of Phe184 and Phe305. **(F)** Comparison of PNK-DNA1 (grey) with the structure of Phosphoserine phosphatase (PDB: 1J97; blue) containing a beryllium fluoride aspartic acid ester (BeF)-Asp11 suggests that we have trapped an ‘end-seeking’ complex, as the indicated phosphate group (5’P-C_5) — that would be a 3’ phosphate in the absence of the C5 nucleoside (dotted circle) — is not in the correct position or orientation for in-line attack by the Asp170 nucleophile.

In this and subsequent figures, all ligands are shown in a ‘ball-and-stick’ representation, with nitrogen, oxygen and phosphate atoms coloured blue, red and pink respectively. A purple sphere represents a magnesium ion (or manganese where indicated). Potential hydrogen bonds, where shown, are indicated by a black dotted line. All secondary structure elements, where labelled, are according to the nomenclature of (Bernstein et al., 2005). Figures were generated using either QtMG (Potterton et al., 2004) or MacPyMOL (Delano, WL).

See also Figure S1.

Europe PMC Funders Author Manuscripts

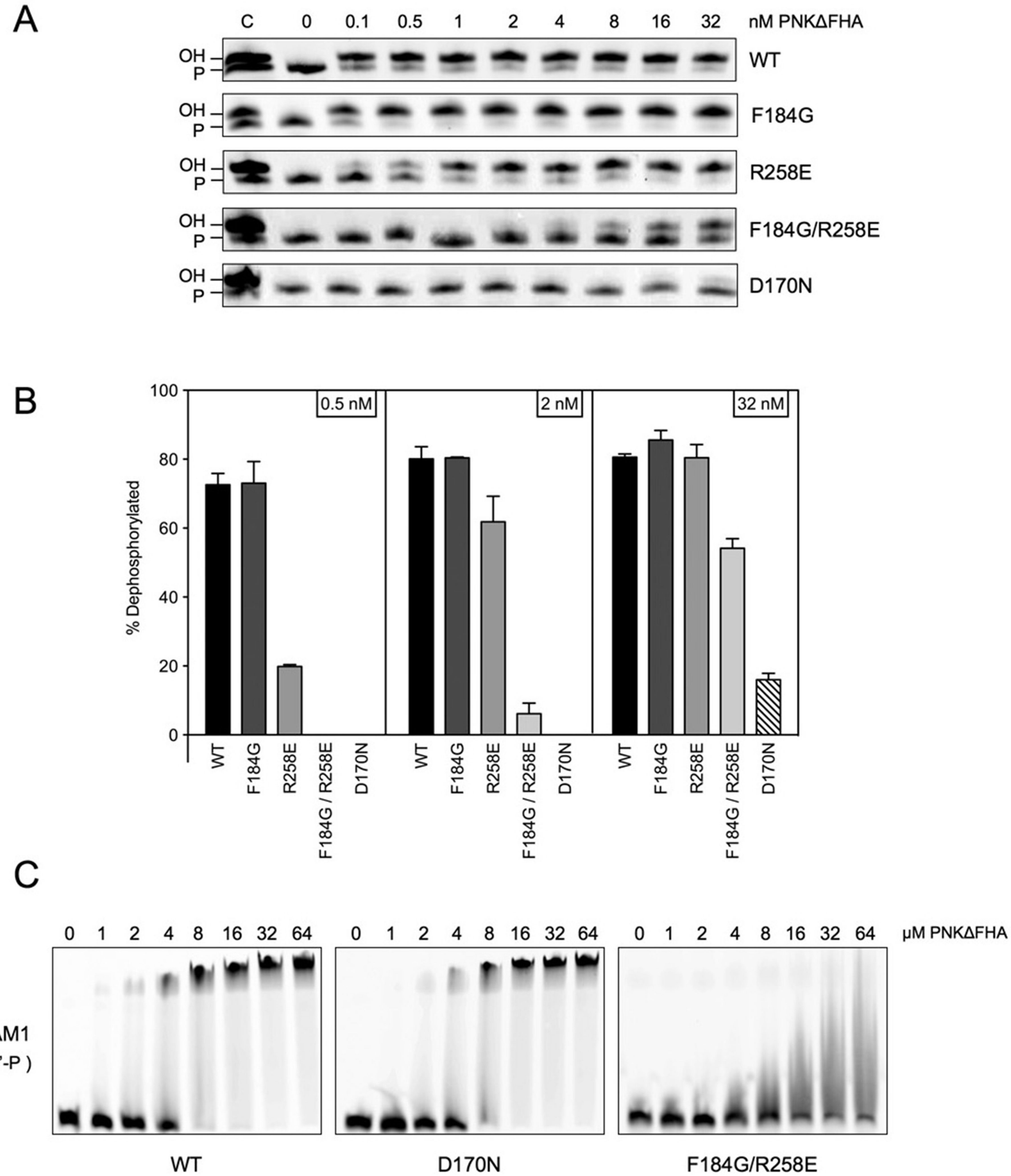

Figure 2. Mutational analysis of the phosphatase domain

(A) Increasing concentrations of wild-type (WT) or mutant PNKΔFHA were incubated with a fluorescently labelled single-stranded oligonucleotide (FAM1). The enzymatic activity of each protein was judged by its ability to remove a 3'-phosphate from the input oligonucleotide, thereby resulting in a reduced electrophoretic mobility on denaturing polyacrylamide gels. Control lanes (labelled 'C') contain two oligonucleotides, with (P−) and without (OH−) a 3'-phosphate, marking the migration positions of the substrate and product of the enzyme reaction respectively. **(B)** The percentage of dephosphorylated oligonucleotide, at the indicated enzyme concentration, was quantified by fluorimagery. Data presented in each bar chart are the average of at least 3 experiments, with error bars representing 1 standard deviation. **(C)** Representative gel images of electrophoretic mobility shift assays, using wildtype (WT) or mutant PNK (as indicated), with the FAM1 oligonucleotide.

Europe PMC Funders Author Manuscripts

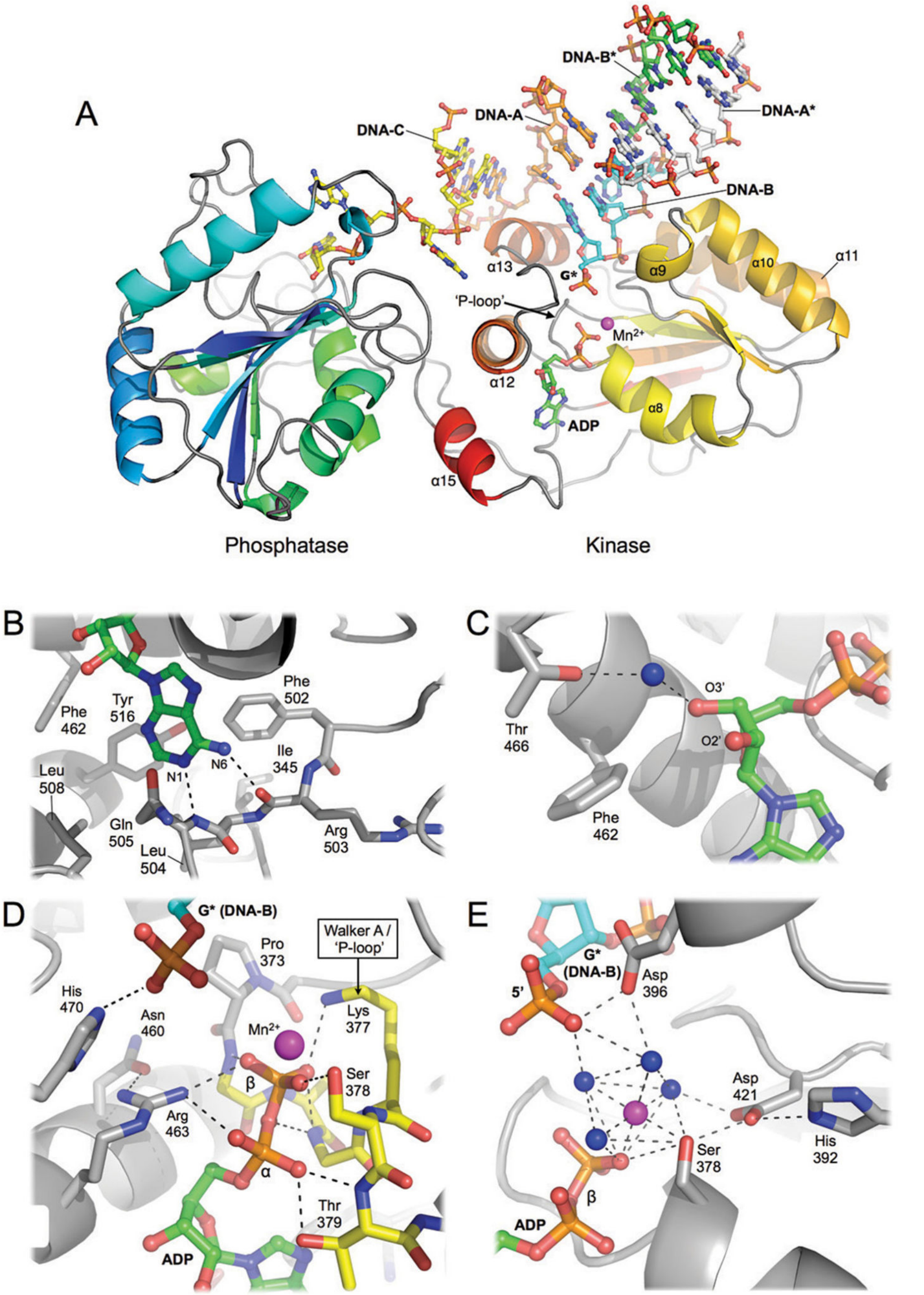

Figure 3. Structural details for ADP-Mn^{2+} and DNA bound to the kinase domain

(A) Secondary structure cartoon representation of PNK-D170N, coloured blue → red from the visible N → C-terminus, highlighting the position of bound ADP (carbon atoms coloured green), a manganese ion (purple sphere) and five annealed 5'-GTCAC-3' oligonucleotides (PNK-DNA2). DNA-A* (carbons atoms coloured grey) and DNA-B* (green) form a self-complementary blunt-ended duplex with a central C:C mismatch, which is stacked against a nicked duplex, with a central T:T mismatch, formed by DNA-A (brown), DNA-B (cyan) and DNA-C (yellow). The 5'-end of each oligonucleotide has been

phosphorylated during crystallogenesis — with the concomitant turnover of ATP — producing a product complex where the 5’-end of DNA-B (labelled G*) is in close proximity to the active site of the kinase domain. **(B)** Details of the observed ‘hinge’-binding mode for ADP, highlighting the interactions of the adenine ring with the backbone carbonyl and nitrogen of residues Gln505 and Arg503 respectively. **(C)** A water-mediated interaction of Thr466 with the ribose group of ADP. **(D)** Residues of the ‘P-loop’ make multiple electrostatic interactions with the diphosphate tail. The 5’-phosphate of DNA-B (G*) also receives a hydrogen bond from the side-chain of His470. **(E)** Coordination of the manganese ion though direct interaction of the Ser378 side-chain, with four water molecules and the β-phosphate of ADP serving to complete the octahedral coordination.
See also Figure S2.

Europe PMC Funders Author Manuscripts

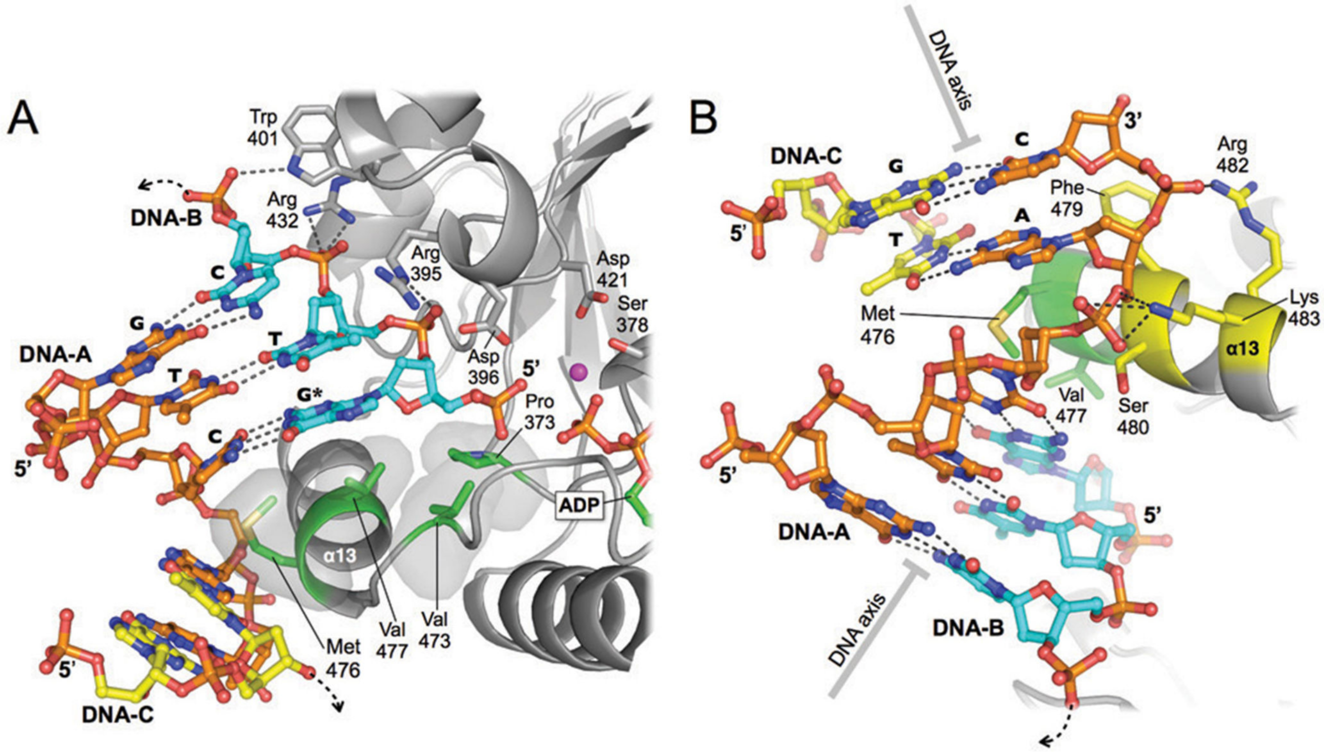

Figure 4. Recognition of Strand Discontinuity by PNK

(A) The three nucleotides at the 5' end of DNA-A (carbon atoms coloured orange) are fully base-paired to the 5'-phosphorylated guanine of DNA-B (G*, carbon atoms coloured cyan) plus the following 2 bases, with a central T-T mismatch. Residues Arg395, Trp401 and Arg432 contact the phosphate backbone of DNA-B. The exposed face of the G*-C base-pair is packed against a hydrophobic surface provided by the side-chains of Pro373, Val473, Met476 and Val477 from α-helix 13 (Van der Waals radii are indicated by the grey envelope surrounding each amino acid). In order to improve the clarity of the figure, some nucleotides are not shown. **(B)** The 2 remaining bases of DNA-A are base-paired to the 5'end of a third oligonuceotide (DNA-C; yellow) to produce a nicked-DNA substrate. The exposed face of the A-T base-pair is packed against a hydrophobic surface provided by the side-chains of Met476, Phe479 and Ser480 (again contained within α-helix 13) with residues Arg482 and Lys483 providing polar interactions with the phosphate backbone. The backbone of the continuous strand (DNA-A) also undergoes a substantial change in direction due to the presence of the inserted helix.

See also Figure S3.

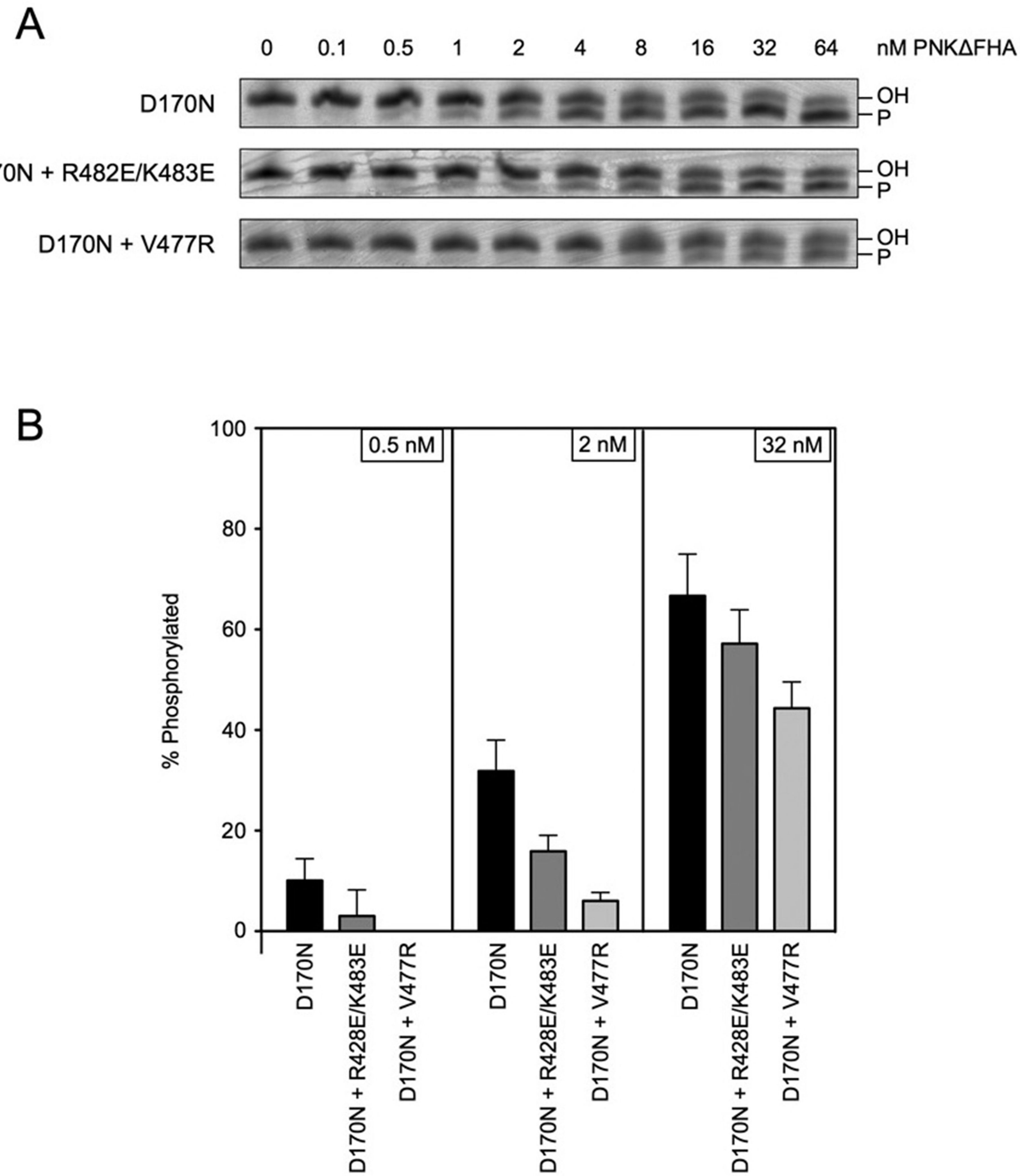

Figure 5. Mutational analysis of the kinase domain

(A) Increasing concentrations of PNK-D170N or the indicated mutant were incubated with a fluorescently labelled nicked-DNA substrate. The enzymatic activity of each protein was judged by its ability to add a 5’-phosphate to the input DNA (−OH), thereby resulting in an increased electrophoretic mobility on denaturing polyacrylamide gels (−P). **(B)** The percentage of phosphorylated substrate, at the indicated enzyme concentration, was quantified by fluorimagery. Data presented in each bar chart are the average of at least 3 experiments, with error bars representing 1 standard deviation.

See also Figure S4.

Europe PMC Funders Author Manuscripts

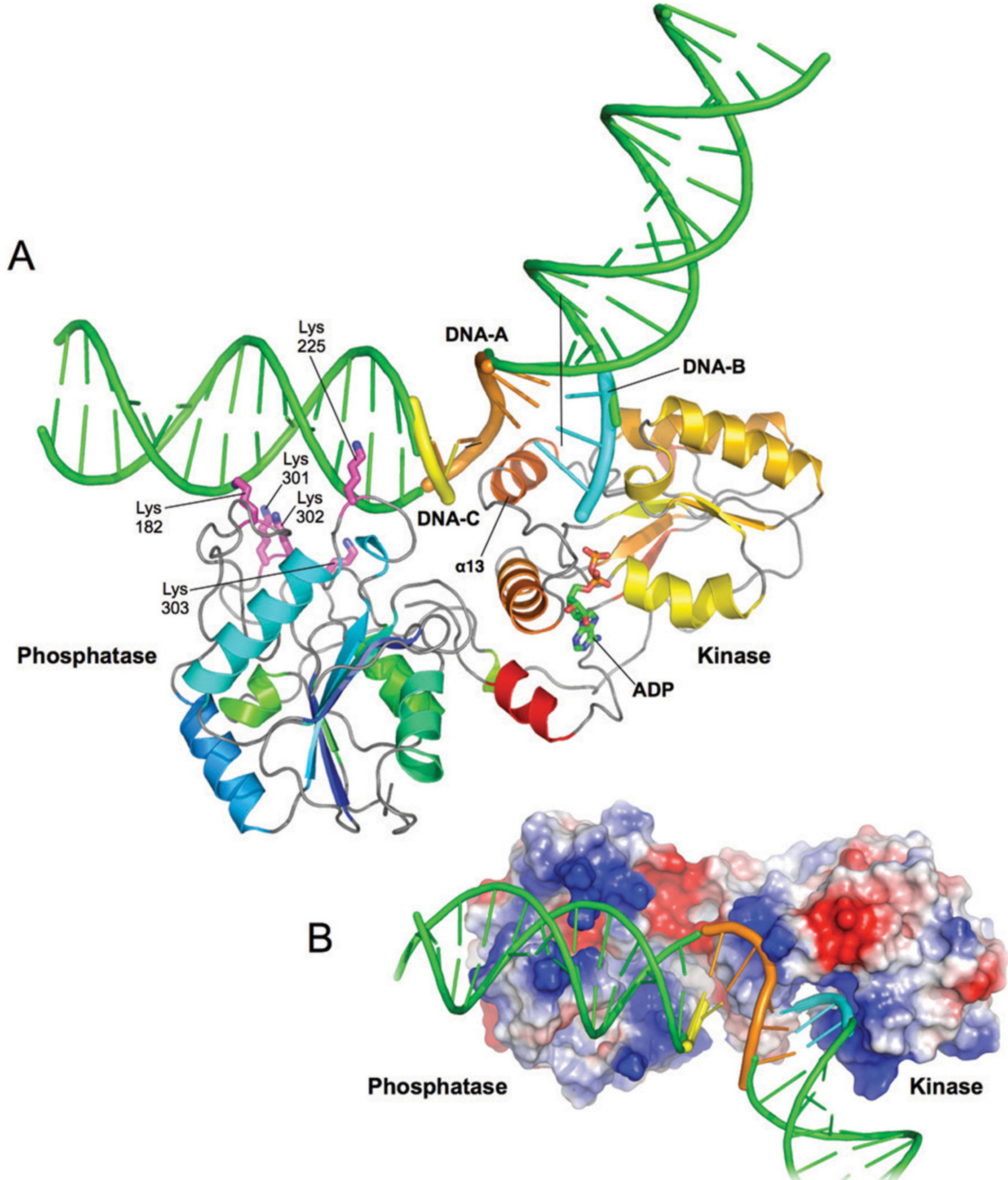

Figure 6. Binding of extended DNA substrates to PNK

(A) A model for binding of a an extended nicked-DNA substrate to PNK — productively engaged with the kinase domain — was generated using the five ‘GTCAC’ oligonucelotides as positioning markers for the placement of two ideal, B-form DNA duplexes (coloured green). The extended DNA is bent by ~ 70° by its interaction with the PNK. The indicated lysine residues (shown as magenta coloured sticks) presented on the surface of the phosphatase domain are favourably positioned to provide electrostatic interactions with the phosphate-backbone of the modelled DNA substrate — thereby suggesting that the phosphatase domain may play a role in assisting the kinase domain in its activity towards nicked and gapped DNA substrates.

(B) A rotated view of the model, showing a molecular surface for PNK coloured according to electrostatic potential, from blue (basic, positive charge) through to red (acidic, negative charge). The path of the nicked-DNA substrate positions the phosphodiester backbone to interact favourably with regions of positive charge on the surface of both the phosphatase and kinase domains.

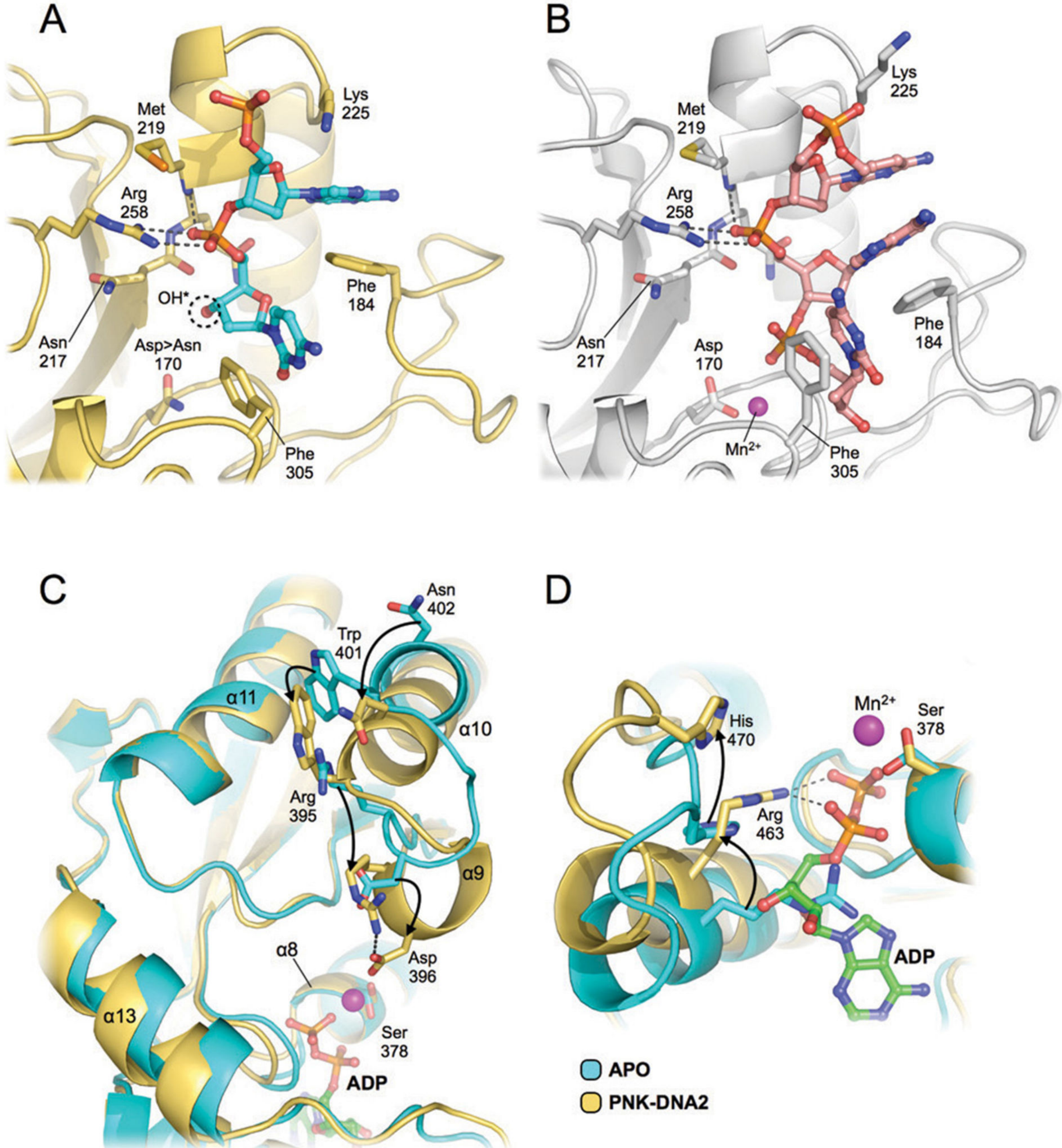

Figure 7. Structural plasticity within the phosphatase and kinase domains of PNK

Comparison of single-stranded DNA bound to the phosphatase domain in the (A) PNK-DNA2 and (B) PNK-DNA1 crystal structures. In both cases, Arg258 and the backbone nitrogen of Met219 interact with the phosphate backbone of the bound oligonucleotide, with Lys225 and Phe184 providing stacking interactions with either one or two of the incoming bases — facilitated by the structural plasticity of the loop containing Phe184 — and with the 3'-terminal nucleotide stacking against Phe305. The position of the ribose sugar hydroxyl in (A) — marked as OH* — suggests that if a 3' phosphate were present, it would be able to

Europe PMC Funders Author Manuscripts

interact productively with the active site of the enzyme. See also Figure S5. Panel C and D show the superimposed structures of the kinase domain from the unliganded ‘apo’ (cyan) and ADP-Mn^{2+} (yellow) bound forms of PNK. (C) Helices α9 and α10, along with β-sheet 16 and interconnecting loops, undergo a structural rearrangement upon binding to DNA and ADP, swinging towards the centre of the protein — resulting in positional rearrangements of the side chains Asn402, Trp401, Arg395 and the catalytic Asp396. (D) A more subtle rearrangement also occurs in the loop carrying amino acid His470, due to the interaction of Arg463 with the diphosphate tail of ADP.

Europe PMC Funders Author Manuscripts

Table 1
Data collection and refinement statistics

	PNK-APO (3zvl)	PNK-DNA1 (3zvm)	PNK-DNA2 (3zvn)
Data collection ‡			
Space group	$P2_1$	$P2_1$	$P2_12_12_1$
Cell dimensions			
a, b, c (Å)	42.8, 63.5, 67.9	44.9, 75.2, 135.2	69.3, 73.0, 114.4
α, β, γ(°)	90, 91.8, 90	90, 96.3, 90	90, 90, 90
Resolution (Å)	33.9 – 1.65 (1.74-1.65)*	38.9 – 2.00 (2.1-2.0)	36.5 – 2.15 (2.27-2.15)
R_{merge}	0.07 (0.572)	0.12 (0.31)	0.11 (0.657)
Mean $I/\sigma I$	13.1 (2.3)	9.32 (3.5)	8.5 (2.3)
Completeness (%)	90.1 (58.8)	99.8 (98.5)	90.4 (92.7)
Redundancy	3.6 (3.4)	5.1 (3.8)	4.3 (4.4)
Wilson B (Å^2)	14.97	15.22	32.14
Refinement			
Resolution (Å)	33.9 – 1.65	38.5 – 2.00	36.5 – 2.15
No. reflections	76395	60655	28753
R_{work} / R_{free}	0.17 / 0.22	0.15 / 0.20	0.20 / 0.26
No. atoms	3536	7431	3688
Protein	2969	5975	
Ligand/ion	16 (acetate)	8 (acetate)	27 (ADP)
	4 (Cl^-)	54 (ADP)	491 (DNA)
	36 (glycerol)	116 (DNA)	12 (glycerol)
	1 (Mg^{2+})	48 (glycerol)	1 (Mn^{2+})
		30 (HEPES)	
		4 (Mg^{2+})	
Water	510	1196	253
B-factors (average)			
Protein	18.8	16.0	46.36
Ligand/ion	30.9 (acetate)	33.1 (acetate)	31.64 (ADP)
	33.0 (Cl^-)	11.6 (ADP)	43.35 (DNA)
	27.4 (glycerol)	30.7 (DNA)	49.8 (glycerol)
	9.8 (Mg^{2+})	24.1 (glycerol)	27.3 (Mn^{2+})
		32.6 (HEPES)	
		9.0 (Mg^{2+})	
Water	32.0	29.1	43.62
R.m.s. deviations			
Bond lengths (Å)	0.006	0.007	0.007
Bond angles (°)	1.026	1.099	1.258
Model Quality			
Rotamer outliers	4 / 305	4 / 634	7 / 302

	PNK-APO (3zvl)	PNK-DNA1 (3zvm)	PNK-DNA2 (3zvn)
Ramachandran outliers	0 / 377	1 / 755	0 / 374
Ramachandran favoured	370 / 377 (98.1%)	745 / 755 (98.7%)	362 / 374 (96.8%)

‡Data were collected from a single crystal in each case.

*Values in parentheses are for highest-resolution shell.

Europe PMC Funders Author Manuscripts